Mass Flow Rate Control of Solenoid-Based Injectors

International Journal of Engine Research
():1–10

DOI
www.sagepub.com/
SAGE

Muhammad Sarmad Qureshi [1] Burhan Kara [2] Özgür Ertunç [2] Özkan Bebek [2]

Abstract

This paper presents a mass flow rate control method for solenoid-based injectors in open-loop, i.e. without physical sensor feedback. Measuring the mass flow rate in injectors is important because the performance of the injector determines fuel consumption and emissions. While it is possible to perform this control using different types of sensors, this would increase the cost and reduce the reliability. With this study, it was aimed to control the mass flow rate of solenoid-based injectors using continuous switching control to regulate the injector's needle displacement without using sensors. For this purpose, a solenoid-actuated injector prototype was created. Model-based estimators were used to determine the states of the injector, while a super-twisting sliding mode controller was used to track the desired mass flow rate references. The results of the experiments showed that tracking for sinusoidal, triangular, and square trajectories yielded a mass flow rate percent error of less than 1.06. The proposed open-loop control algorithm can be used to track different mass flow rate references in internal combustion engines.

Keywords

Mass Flow Rate Control, Open-loop, Super-twisting Sliding Mode Control, High gain observer, Solenoid actuator.

Introduction

The industry has been forced to investigate novel ideas and create new technologies for cost-effective engines with reduced fuel consumption and exhaust emissions, particularly for internal combustion engines. Such new technology is important to maintain a competitive advantage in the industry. One of the parts that can reduce the cost of engines is the injector. However, cost reduction in injectors is challenging as it might lead to the engine not meeting the performance requirements, which are determined by the atomization quality and precise amount of the injected liquid.[1] The former depends on the droplet size and spray cone angle, while the latter depends on controlling the needle movement that regulates the spray quantity. When the needle movement is controlled, only the injection timing is followed, and the amount of sprayed fuel is not fully controlled. It is possible to increase the engine efficiency by controlling the mass flow[2,3] rather than the needle movement because doing it allows the injection of an exact amount of fuel. Currently, mass flow controllers are used for purposes such as urea dosing to eliminate hazardous gases from diesel engines,[4] gas dosing into bioreactors for bacterial growth,[5] and creating different gas or liquid mixtures for different chemical reactions.[6]

A solenoid-based injection system can be considered a cost-effective solution, which can be used to flexibly control and regulate the injection quantity based on desired operating conditions. The solenoid actuator of the injector and its controller regulates the operation and are one of the main factors determining the desired performance of an internal combustion engine. The performance can be improved by using the information from any sensors to be added to the injectors. However, it is hard to check the position of the needle[7], as sensors are not attached to these injectors because of their cost and reliability issues. There are some studies that investigated the position control of solenoid actuators with and without sensors,[8,9] however, these controllers cannot suffice to achieve a robust mass flow rate control because solenoid-based injectors are controlled by continuous switching, and the flow behavior from the needle position cannot be predicted due to nonlinearities and other uncertainties in the system.

Another important factor to consider is the type of actuator used. Piezoelectric actuators are widely used in injectors as they provide a small mechanical displacement at high speed and precision. Hence, more research on mass flow rate control has been done by changing the operating voltage of piezoelectrically operated injectors.[10,11] Also, the injection efficiency was improved by utilizing a model-based approach to estimate the parameters of the piezoelectric actuators that control the injection process.[12] Due to the discrete nature of electromagnetic solenoid actuators, which are widely used as an alternative to piezoelectric actuators, displacement can be controlled using continuous switching control. But doing this robustly without using a sensor is challenging. Therefore, this article proposes a method for mass flow rate control of solenoid-based injectors by regulating the needle displacement.

[1]Department of Electrical & Electronics Engineering, Özyeğin University, Istanbul, 34794 Turkey
[2]Department of Mechanical Engineering, Özyeğin University, Istanbul, 34794 Turkey

Corresponding author:
Özkan Bebek
Email: ozkan.bebek@ozyegin.edu.tr

In order to control the combustion process more effectively, it is necessary to investigate the fuel injection phenomenon.[13] The fundamental challenge in combustion control is to accurately determine the opening and closing times of the injectors. The complex electrical, hydraulic, and mechanical operations that take place inside a fuel injector happen fast, making it challenging to calculate the opening and closing times of the nozzle.[14–16]. Generally, it is assumed that the electrical control pulse being sent to the coil marks the start of the injector opening.[17,18] However, the dead zone time of the solenoid inside the injector prevents direct connections between the applied pulse-width modulated voltage and the injector needle position, making this determination error-prone. As a result, it is hard to achieve the desired mass flow rate. Many of the control systems found in the literature that are used to control the needle's position use sensory feedback. Utilizing a current-detecting device that can track current variations and, as a result, determine instances a solenoid actuator closes and opens.[19] Lillington et al.[20] emphasizes accurate modeling and simulation in complex electro-mechanical system design. Accurate models improve system performance and reliability while reducing development and testing time and cost. The injector's performance was studied and optimized using the model. The position control of a pneumatic cylinder using the PWM control method to control the mass flow rates of the injector, but only for the on-off case, has also been studied.[21]

To the best of our knowledge, there are no other studies in the literature focusing on an indirect control of the mass flow rate by controlling the exact position of the injector's needle in a sensorless environment. This study bridges this gap in the literature by focusing on the design and construction of a novel cost-effective solenoid-based injector prototype, as an alternative to the ubiquitous piezo-electric injectors, to control the mass flow rates in an open-loop environment. Using the developed prototype, experiments were carried out to determine respective mass flow rates based on the orifice area control. Specifically, it was aimed to regulate the mass flow rates using an open-loop controller, while monitoring the effects of the structural elements. The experiments were done using a benchtop solenoid-based injector. The results of the experiments showed that the proposed control method and the designed injector is operable, forming a basis for similar other injectors to be developed for use in the automotive industry.

In the following section, the proposed injector system is explained followed by an explanation of the proposed control algorithm. Then the different desired mass flow rate reference signals are briefly discussed. Finally, the experimental results and conclusions are presented.

Pintle-type Solenoid Based Injector

In this study, a cost-effective prototype of a solenoid-based injector was designed and built to examine the mass flow rate control problem. A benchtop setup, consisting of a solenoid actuator, spring, pintle-type atomizer, and an encoder assembly was used (see Figure 1). A pintle-type injector was selected to be used considering their usage in the high flow rate applications.[22] Characteristics of the injector are given in Table 1. Since a cost-effective and exact measurement of the flow rate was unattainable, a load cell was used to measure the flow over a specified time. A linear encoder was built using a linear rail and a rotational encoder, with a pulley-string system. The linear encoder assembly was attached to the non-injecting side of the injector, adjacent to the solenoid actuator, which was used to verify the adequacy of the applied control algorithm.

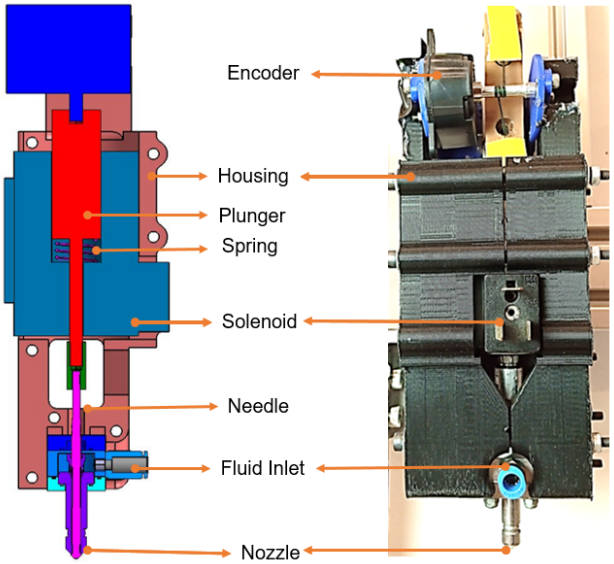

Figure 1. The cut view (left) and built hardware (right) of the injector prototype to evaluate the control algorithm are shown. The needle is attached to one side of the solenoid's plunger; the linear encoder is attached to the other side of the solenoid's plunger.

Control algorithm design

This section provides a summary of the control methodology, followed by the modeling approach and design of the control algorithm to reach the desired mass flow values.

Methodology

A valid mathematical model for the injector can be created to determine the mass flow rate without the need for sensors. Instead of sensor measurements, an observer-based estimation can be used to estimate the system states. However, since there is no linear relationship between the solenoid needle displacement (the electromechanical output of the operation) and mass flow rate (physical output of the injector), a calibration method must also be developed to establish a relationship between the two (see Figure 2).

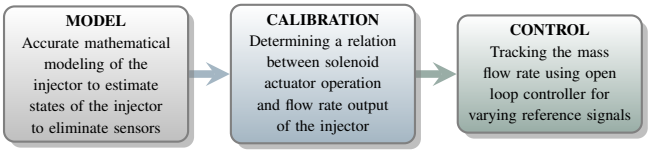

Figure 2. The overview of the control methodology to develop the sensorless mass flow rate control of solenoid-based injectors

Table 1. Properties of a Pintle-type Injector with Solenoid Actuator

Parameter	Description	Unit	Value
Injection Pressure	Pressure at which fluid is injected	bars	6
Maximum Flow Rate	Rate of fluid flow through the injector	g/s	9.8
Materials	Materials used to construct the injector	–	Stainless steel, ABS
Nozzle Size	Size of the nozzle through which fluid is injected	mm	2
Orifice Diameter	Diameter of the orifice through which fluid flows	mm	1.75
Sealing Type	Type of sealing mechanism to prevent leaks	–	Static, dynamic
Plunger Mass	Mass of the plunger that moves the fluid	g	91.32
Spring Constant	Stiffness of the spring used to inject the fluid	N/m	420
Solenoid Voltage	Voltage required to operate the solenoid	V	24
Coil Resistance	Electrical resistance of the solenoid coil	ohms	46.1
Coil Turns	Number of turns in the solenoid coil	turns	2900
Solenoid Stroke	Distance the solenoid moves when in operation	mm	4

With the aim of developing a control approach to achieve the desired mass flow rates and tracking any desired reference profile, a simulated model and an observer were used to track the desired trajectories and achieve desired mass flow rates. While constructing this approach, a closed-loop position control algorithm was used to get the transformation function for the mass flow rate to the needle position. The transformation function mentioned will serve as the calibration of the injector, allowing the relationship between the solenoid needle displacement and the corresponding mass flow rate to be accurately determined. An evaluation of this approach was made by assessing the mass flow rate tracking performance of the open loop controller for various reference signals.

Injector electromechanical model

The electrical model: When a solenoid is powered by an input voltage v_{0r}, the electromagnetic force (F_{em}) generated in the injector attracts the plunger. Figure 3 shows the forces acting on the injector when this happens.

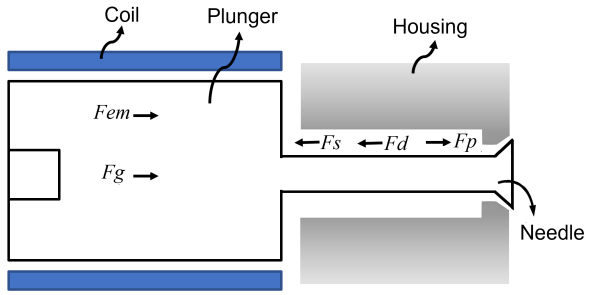

Figure 3. The force analysis model of the injector. F_g, F_{em}, F_d, F_s, F_p, are the gravitational, electromagnetic, damping, spring, and water pressure forces, respectively.

In the electrical model, the input voltage is represented by (1).

$$v_{0r} = R_r\, i_r + \frac{d\lambda_r}{dt} \tag{1}$$

where, λ_r is the total flux, i_r is the coil current, and R_r is the coil resistance. Here λ_r is represented by (2).

$$\lambda_r = L_r\, i = L(x) i_r \tag{2}$$

where L_r is the solenoid's inductance.

The voltage and coil current of the solenoid is derived from the combination of (1) and (2), as in (3):

$$v_{0r} = R_r \cdot i_r + L(x) \cdot \frac{(di_r)}{dt} + i_r \frac{dL(x)}{dx} \cdot \frac{dx}{dt} \tag{3}$$

$$\frac{di_r}{dt} = \frac{1}{L(x)} \left[v_{0r} - R_r i_r - i_r \frac{dL(x)}{dx} \frac{dx}{dt} \right] \tag{4}$$

The current calculated from (4) is used to calculate the electromagnetic force, as in (5):[23]

$$W'_m(i_r, x) = \int \lambda(i_r, x) di_r = \int L(x) i_r di_r = \frac{i_r^2 L\,(x)}{2} \tag{5}$$

$$F_{em} = \frac{\partial W'_m\,(i_r,\ x)}{\partial x} = \frac{1}{2} i_r^2 . \frac{dL\,(\,x)}{dx} \tag{6}$$

where, $W'_m(i_r, x)$ is a function of inductance and coil current, which is called co-energy. The injector inductance is represented by its relationship with the total reluctance $\Sigma_n \mathcal{R}_{ri}$ and number of coil turns (N_r) as (7):

$$L(x) = \frac{N_r^2}{\Sigma_n \mathcal{R}_{ri}} \tag{7}$$

The mechanical model: Based on the force analysis model of the injector shown in Figure 3, a mechanical model was built using Newton's second law to describe the plunger motion, which is described below:

$$\Sigma F = m_p \frac{d^2x}{dt^2} \tag{8}$$

$$F_{em} + F_p + F_g + F_d - F_s = m_p \frac{d^2x}{dt^2} \tag{9}$$

$$F_{em} + P_{in} S_o - m_p a_g - b_r \frac{dx}{dt} - k_r(x + \Delta) = m_p \frac{d^2x}{dt^2} \tag{10}$$

where, F_g, F_{em}, F_d, F_s, F_p, Δ, k_r, b_r, P_{in}, m_p, x, and S_o, are the gravitational force, electromagnetic force, damping force, spring force, the force caused by water pressure, precompression of the spring, spring stiffness, damping coefficient, inlet water pressure, plunger mass, plunger displacement, and orifice cross-sectional area of the injector system, respectively.

The purpose of this electromechanical model of the injector was to find the relation between the applied voltage and the resulting needle displacement.

High gain observer for velocity estimation

A High Gain Observer (HGO) is a type of observer used in control systems to estimate the unmeasured states of a system. The unique feature of the HGO is that it uses high-gain feedback to magnify the effects of small estimation

errors, thereby improving the accuracy of the estimation. Specifically, the HGO works by combining the system model with the available measurements to form an estimation of the unmeasured states. The HGO is particularly useful in applications where accurate state estimation is needed, and also where the system model is reasonably accurate but measurement noise is present.

The controller of the solenoid actuator requires both position and velocity information of the injector's needle. For the closed-loop control, the needle position is measured using the encoder; for the open-loop control, the simulated model was used. Velocity could be obtained using numerical differentiation of the position but that would amplify the measurement noise of the system. Therefore, HGO was implemented to estimate the velocity output.[24,25]

The HGO provides a suitable and simple solution for nonlinear systems like this one, because it doesn't involve any differential equations. Another advantage it brings is semi-global or global stability,[26] which implies they can ensure stability for any initial condition. The HGO was also preferred due to its easy gain adjustment by pole placement and minimal system-destabilizing peaking effects.[27] In order to get the best performance of the HGO in both the closed- and the open-loop control systems, gain values were tuned heuristically through experimental trial and error. The gains were tuned so that the tracking error and the overshoot would decrease. Equations explaining the observer dynamics are given in (11), (12) and (13).

$$\hat{x}\left[k+1\right] = \hat{v}\left[k\right] + \beta_1\left(z\left[k\right] - v\left[k\right]\right) \tag{11}$$

$$\hat{v}\left[k+1\right] = \Phi_0\left[\hat{y}, u\right] + \beta_2\left(z\left[k\right] - v\left[k\right]\right) \tag{12}$$

$$z = \hat{v}\left[k\right] \tag{13}$$

where, $\hat{x}$ is the estimated position of the needle, and $\hat{v}$ is the estimated velocity of the needle. The gains β_1 and β_2 were empirically tuned following the guidelines provided by Khalil and Grizzle,[28] until the error was minimized in the output following the design criterion of $\beta_2 >> \beta_1 >> 1$. Thus, β_1 and β_2 were assumed as 27 and 294, respectively.

Super-twisting sliding mode control (STSMC)

Supertwisting Sliding Mode Control (SMC) is a non-linear control algorithm used in control systems to track reference signals and reject disturbances. The unique feature of STSMC is that it uses a sliding surface to generate control inputs that drive the system states to follow the reference signal, while also compensating for external disturbances. Specifically, the algorithm involves the use of a sliding surface that represents the error between the system states and the desired reference signal and a set of control laws that are designed to force the system states to converge to the sliding surface and then follow it towards the reference signal.

The SMC algorithm is enhanced by the addition of a supertwisting term, which improves the tracking performance by reducing the chattering effect, a common issue in traditional sliding mode control. The supertwisting term provides a smooth control input and results in a faster convergence to the sliding surface, while also reducing the tracking error.

The STSMC algorithm is particularly useful in applications where high tracking accuracy is required, and where the system model is subject to external disturbances and uncertainties.[29]

Since there are a lot of nonlinear forces acting on the system, the controller had to be robust and versatile in order to follow the desired reference signal. Also, physical systems like this can be subject to external disturbances that may degrade control performance or even cause the system to become unstable. Motion tracking with super-twisted sliding mode control (STSMC) is found to be successful in nonlinear motion control systems with external interference and system uncertainties.[7,9,30,31] Therefore, this control approach was also applied here.

In STSMC, system states are used to reduce tracking error. In this study, the injector needle position and velocity were used as feedback. The needed state information was acquired from the simulated system model and the high-gain observer as there was no sensor feedback. In order for the applied controller to be successful, the data from these estimators had to be of good quality.

First-order sliding surfaces, which are frequently used in the literature, were chosen as the sliding surface for the sliding mode controller.[32] In addition, similar performances were attained when the first-order and higher-order sliding surfaces were compared. So, first-order sliding surfaces were used in the controller to minimize the computational effort. STSMC gains were empirically tuned for both closed-loop and open-loop systems. The range of the gains was chosen heuristically by experimental trial and error. The controller aimed to reduce the error between the desired and actual mass flow rate of the injector. Gains were increased while tracking the desired input trajectory in order to reduce overshoot, undershoot, and system lag while decreasing the tracking error.

The sliding surface S of STSMC is defined as:

$$S = \frac{\mathrm{d}e}{\mathrm{d}t} + ce \tag{14}$$

where e is the error between the desired and measured output, c determines the position of the unique pole of reduced dynamics of the system when the system is in the sliding phase. As soon as the trajectories of the controlled system reach the sliding surface, the system does not require model parameters.

After the design of the sliding manifold, a control output is required which keeps the system trajectories onto the sliding surface and is defined as in (15)

$$U = -u \cdot sat\left(S\right) \tag{15}$$

where,

$$U = \begin{cases} -u & S < 0 \\ u & S > 0 \end{cases} \tag{16}$$

u can be arbitrarily chosen sufficiently large constant until the desired output is achieved. For the simulation, the controller gains S and u were empirically tuned as 52 and 17, respectively. Gains were tuned to 44 and 31 for the hardware experiments. First-order sliding surfaces, which are frequently found in the literature, were chosen as the sliding surface.[32] First-order sliding surfaces were utilized

to minimize the computing effort after higher-order surfaces were investigated and found to perform comparably.

Experimental setup

As this study focuses on the automobile industry and developing an open-loop mass flow rate control for solenoid-based injectors, a control system was developed (with a sampling rate of 1 kHz) with the capabilities of an Electronic Control Unit (ECU) used in automobiles to replace this unit.

In the experiments, a solenoid actuator that ran on 24 VDC, coupled to a pintle-type needle on one end and a linear encoder to the other end (see Fig 1), was used. The experimental devices and their connections are shown in Figure 4. A USB data acquisition system (DAQ) comprised of a Quanser Q8 board supported by the MATLAB Simulink, which produces 16-bit analog output control signals, was used to create the control signal for the injector. Since the DAQ board can only support currents up to 20 mA at 10 V, which is insufficient for the injector, the DAQ output was amplified using a National Instruments CompactRIO (NI cRIO) system. The DAQ signal was acquired by a 12-bit analog input module (NI9201) attached to the NI cRIO, which was then transformed into an equivalent PWM signal in embeded LabView software. A digital I/O module (NI9472) attached to the NI cRIO transmitted the amplified 24 V PWM signal to the EM solenoid actuator.

The position data were collected by a Broadcom HEDS5645-I13 rotary encoder through a pulley-string mechanism. This encoder provided 2048 counts per revolution with quadrature reading. The single increment of the encoder corresponded to a linear displacement of 6.584 μm.

In order to track the injection's intended mass flow,a FUTEK load cell with a resolution of 0.001 g was used to measure the injected mass of the fluid. All tests were completed in a test bench environment using water at 6 bar pressure.

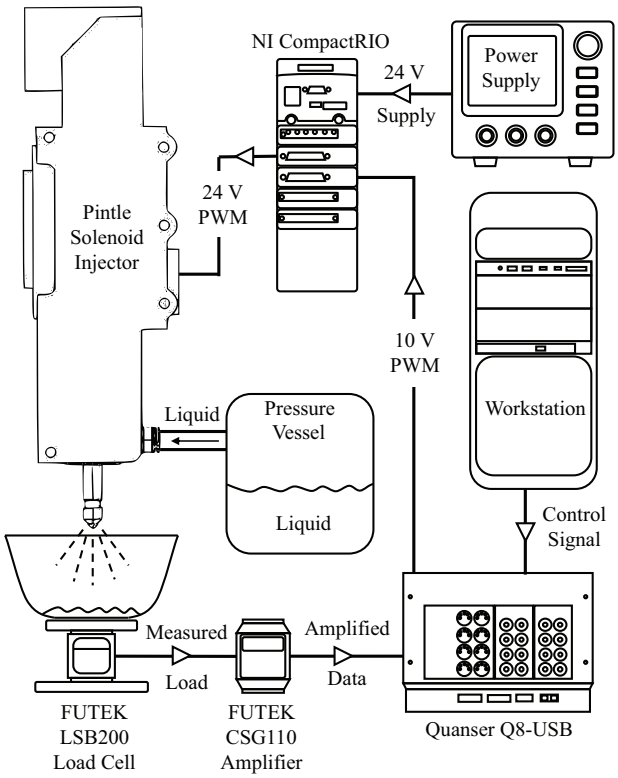

Figure 4. The experimental setup and the main components of the benchtop injection system.

Mass Flow Rate Control

Measurement Of Flow Rate Using Closed Loop Control

The aim of the closed-loop control was to measure how much needle opening corresponds to how much mass flow rate. Such relation would depend on the flow, pressure, fluid type, nozzle type and size, as well as the needle displacement. Also, the relationship could be different for each injector.

In experiments, the opening of the injector needle was regulated using STSMC in closed-loop with the needle position as feedback, as shown in Figure 5. The figure shows the control block diagram to determine the system's average mass flow (m). The mass flow rate ($\dot{m}$) and needle position (x) were correlated using load cell data. The load cell's fluid force measurement determines the injector's mass flow rate. STSMC closed-loop regulated the injector needle using needle position feedback. The control approach calculates the system's average mass flow rate by correlating load cell measurement with the injector needle position. The injected water was collected and its weight, m, was divided by the total spray time to get the averaged mass flow rate $\dot{m}$. A look-up table was created with the experimental data by giving discrete signals to the injector and measuring the injected liquid's mass using a load cell (data points are shown in Figure 6). As the experiments were conducted at low water pressures, no water flow was observed for small openings. A linear fit to the data provided a transformation function for the *mass flow rate to needle position*, as given in (17).

$$\dot{m} = 0.123x - 1.663 \tag{17}$$

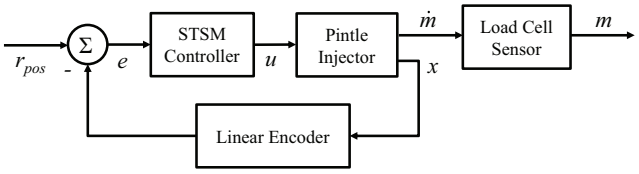

Figure 5. The controller block diagram to determine averaged mass flow, m. The load cell data was used to get the relation between mass flow rate, $\dot{m}$, and needle position, x.

Closed-Loop Mass Flow Rate Control

Once the transformation function for the mass flow rate to the needle position was established, a variety of mass flow rate reference signals were tracked using the closed-loop controller to test the method. The reference mass flow rate signals, r_{mfr}, consisted of various waveform signals with different amplitudes and frequencies to study the adequacy of the method. As the relation between the needle's position and the injector's mass flow rate has already been established,

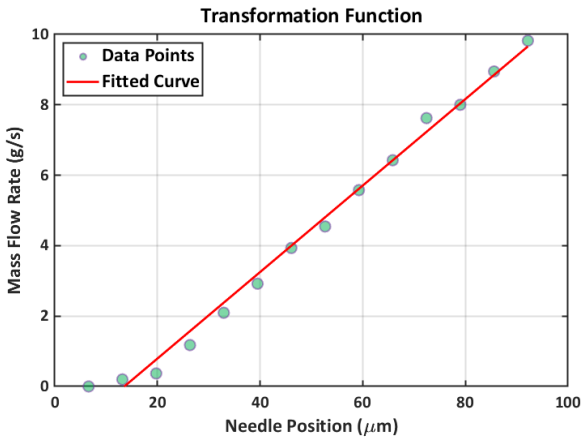

Figure 6. The transformation function for the mass flow control was achieved using the curve fitting approach. The fit does not cross the origin as no flow of liquid was observed for relatively small needle openings.

corresponding needle position, r_{pos}, was tracked for the desired mass flow rate. The implemented control algorithm can be seen in Figure 7. In the closed-loop mass flow rate control system, the encoder was used to measure the actual position of the injector's needle transforming it to the mass flow rate, and the controller compares it to the desired setpoint value. If the measured value is below the setpoint, the controller sends a signal to increase the flow rate, and if it is above the setpoint, the controller sends a signal to decrease the flow rate. The solenoid actuator then adjusts the needle opening controlling the flow rate accordingly. Since sensor information was used in this control method, the results obtained here were accepted as the baseline performance for the sensorless method.

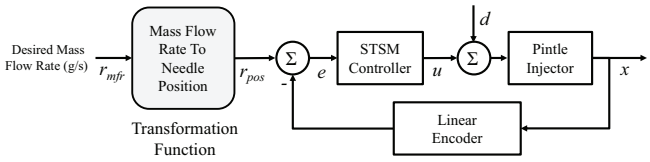

Figure 7. The block diagram of the closed-loop mass flow rate controller is shown. The injector was made to track the reference mass flow rate reference signal using STSMC algorithm, using feedback from the encoder. The control algorithm also incorporates the disturbance d in the system.

Open-Loop Mass Flow Rate Control

As the purpose of this study was to develop a controller that can control the mass flow rate without a sensor feedback, an open-loop position control using the relation between the needle opening and mass flow rate was used, as given in (17).

Looking from the outside, the designed controller acts as an open loop but involves a component within which the controller requires the position and the velocity of the system to close the loop. This open-loop control approach used is shown in Figure 8. Based on this approach, the following three blocks inside the controller were designed. To estimate the position of the needle, $\hat{x}$, a dynamic system model of the injector was created using analytical and experimental methods, which took PWM voltage as the system input, and

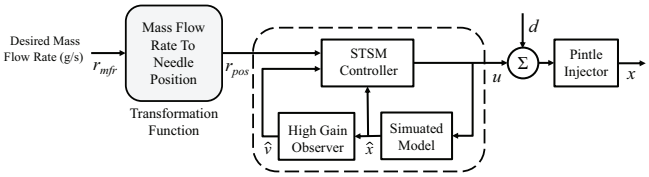

Figure 8. The block diagram shows the open-loop mass flow rate controller. The injector was made to track the reference mass flow rate signal using the STSMC algorithm. $\hat{x}$ and $\hat{v}$ are estimated position and estimated velocity by the simulated model and the HGO, respectively.

the needle position as the system output. An observer was implemented to obtain the noise-free velocity output of the solenoid actuator, $\hat{v}$, hence the needle velocity. An STSMC was designed for effective position tracking of the actuator. The open-loop mass flow rate control algorithm estimates the needle position using a simulated model, where the position of the needle is determined by the control signal sent to the injector. The transformation equation is then used to convert the estimated needle position into the corresponding mass flow rate. This mass flow rate is then compared to the desired setpoint value using a controller. The controller generates an output signal that is proportional to the difference between the desired mass flow rate and the estimated mass flow rate, and sends it to the injector to adjust the needle position to achieve the desired mass flow rate. Since there is no feedback loop to correct any errors or disturbances, the open-loop control system relies entirely on the accuracy of the simulated model, the transformation equation, the selection of controllers, and the state observer.

Experimental results

Position tracking results

Position tracking experiments were conducted to compare the errors of the implemented closed- and open-loop control algorithms. The tracked trajectory profiles consisted of sinusoidal, triangular, and square signals. The selection of the profiles was made by taking into account the distinctive features of each signal. The reasons for choosing these signal types are as follows. The sinusoidal waveform was chosen because it represents the state change of many things in nature. Square waveform pattern was chosen because the injectors in industrial applications and internal combustion engines are mostly used with this pattern. The triangular waveform was chosen because it is used to test the algorithm's response under rapidly changing piecewise linear input. Using these signal profiles, the position amplitudes of 255, 265, 275, and 285 μm and, frequencies of 0.6, 0.8, and 1.0 Hz were tested. All experiments were repeated 10 times for each controller, and the RMS tracking results were tabulated as in Table 2. The standard deviation data were not included in the table as the variance of the results was less than 2% of the mean, indicating that the variation among trials was negligible, and the results were highly reproducible. The highest of the position tracking RMS error was 14.06 μm for the square reference signal. The maximum tracking error of 19.36 μm was seen for 285 μm amplitude and 1 Hz frequency square reference signal.

Table 2. RMS position tracking errors for closed- and open-loop control are tabulated. Experiments were conducted 10 times for each reference type.

RMS Position Tracking Error (μm)		
Signal Type	**Closed-loop**	**Open-loop**
Sinusoidal	9.93	11.36
Triangular	10.09	11.94
Square	13.37	14.06

Table 3. RMS mass flow rate tracking errors for closed- and open-loop control are tabulated. Experiments were conducted 10 times for each reference type.

RMS Mass Flow Rate Tracking Error (mg/s)		
Signal Type	**Closed-loop**	**Open-loop**
Sinusoidal	7.12	9.02
Triangular	7.25	7.31
Square	28.2	37.1

When the RMS position tracking error was larger than 36.81 μm, the mass flow rate control was not achievable.

The results of tracking a sinusoidal, triangular, and square reference position signal for both closed- and open-loop control approaches are provided in Figure 9.

Mass flow rate tracking results

To test the effectiveness of the proposed algorithm, different mass flow rate trajectories were created with varying amplitudes and frequencies. The trajectory profiles consisted of sinusoidal, triangular, and square signals, similar to the position tracking profiles. Using these signal profiles, the mass flow rate amplitudes varied from high 6 g/s, to intermediate 3 g/s, and to low 0.5 g/s whereas, the frequencies varied from high 5 Hz, to intermediate 2 Hz, and to low 0.2 Hz and 0.8 Hz. The highest mass flow rate the used injector could reach was 9.8 g/s at 6 bar water pressure. Also, for frequencies higher than 7 Hz, performance dropped significantly.

The open-loop control algorithm was tested with the reference signals mentioned above using the transformation function between the mass flow rate and needle position. Since the mass flow rates cannot be accurately measured in real-time due to atomization, the time integral of the desired reference flow rate was calculated to determine the mass of the discharged fluid for the duration of the experiment. This total mass reference was then compared to the amount of collected fluid measured with the load cell.

Experiments were also conducted in closed-loop to compare the results of the open-loop control experiments. Again, for each reference signal, experiments were repeated 10 times, and the RMS tracking results were tabulated as in Table 3. The mass flow rate tracking control results for a single case of sinusoidal, triangular, and square are presented in Figure 10. Here, the load cell measurements are also given for both the closed-loop and the open-loop control algorithms.

Discussion of the results

The error rate of the mass flow rate control was less than 1.06% for low amplitudes and frequencies which verified the effectiveness of the algorithm used. This is similar to the error rate reported for piezoelectric actuated injectors, e.g. by [33].

The percent error boxplots for total mass injected under different reference input profiles using the closed- and open-loop control methods are presented in Figure 11. These show the percent deviation of the actual mass flow rate from the desired mass flow rate for 10 repeated tests. Independent-samples *t*-tests were calculated to compare the average percent closed-loop tracking error to the average percent open-loop tracking error for three reference signals, namely, the sinusoidal, triangular, and square. For the sinusoidal reference signal, no significant difference was found ($t(89) = 1.6559, p > .05$) between the closed-loop mean ($m = 0.99633, sd = 0.59613$) and the open-loop mean ($m = 1.1491, sd = 0.64106$). For the triangular reference signal, no significant difference was found ($t(89) = 1.1453, p > .05$) between the closed-loop mean ($m = 1.1559, sd = 0.72364$) and the open-loop mean ($m = 1.282, sd = 0.75385$). For the square reference signal, no significant difference was found ($t(89) = -11.521, p > .05$) between the closed-loop mean ($m = 1.2225, sd = 0.76369$) and the open-loop mean ($m = 1.0863, sd = 0.74043$). The close performance of both control methods confirms the reliability, while the low standard deviation values confirm the repeatability of the simulated system model, HGO's estimation performance, and the implemented open-loop algorithm. The sinusoidal reference produced the least error whereas the square reference signal resulted in the highest.

Some deductions from the results of these experiments are summarized below:

- The control algorithm gains were tuned using the sinusoidal reference. Because when following the sinusoidal signal, the solenoid actuator was not affected by the admittance time delay, also the dead zone effect was limited. This made parameter tuning easy. As a result, for the sinusoidal reference, the closed-loop errors were very similar to the open-loop ones. For the other reference signals, the same controller gains were used, resulting in comparable results.
- At low amplitudes and low frequencies the error between the desired mass and the actual mass for both the closed-loop and the open-loop control are low. The reason is that at low amplitudes and low frequencies the needle of the injector can fully open and close up following the desired mass flow rate amplitude profiles. The small difference between the desired and the actual values is because of the dead zone and the admittance time of the solenoid actuator used. The dead zone time is the time between the applied voltage and the initial movement of the solenoid's plunger, whereas, the admittance time is the time when the input voltage is cut-off until the residual magnetism stays in the solenoid's coil of the injector before the plunger starts to move in the opposite direction. The dead zone region can be seen between the application of input voltage and the needle's first motion, causing a delay in the system's response. Moreover, the limits of the solenoid-based injector depend on these timings; the shorter the time quicker the response of the injector. For the low frequencies and low amplitudes,

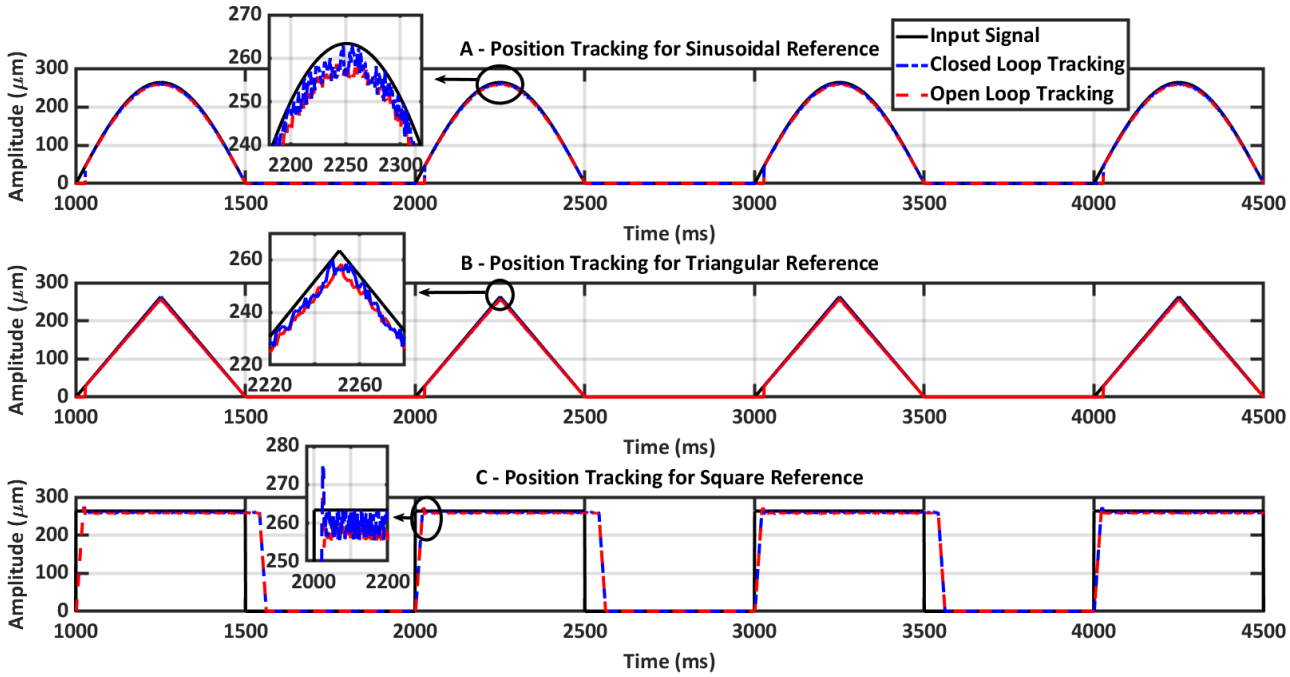

Figure 9. The figures show the results of closed- and open-loop position tracking of signals with a frequency of 1 Hz. A - shows the tracking result for the sinusoidal reference, B - for the triangular, and C - for the square reference signals. Tracking starts once the admittance time is finished.

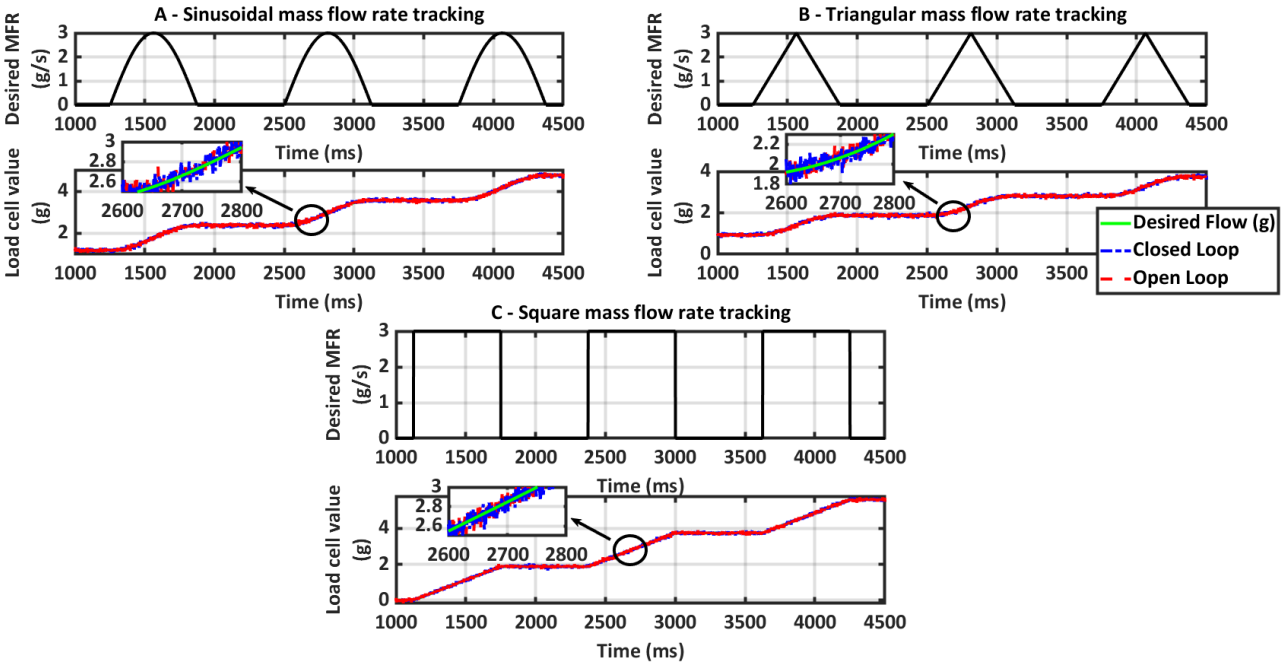

Figure 10. The figures show the results of the mass flow rate tracking for both the closed-loop and the open-loop cases: (A) shows the tracking result for the sinusoidal reference, (B) for the triangular, and (C) for the square reference signals. The case of 3 g/s with 0.8 Hz frequency is shown for reference. The upper plots show the desired MFR reference signals, whereas the bottom graphs show the load cell reading as a comparison of both techniques. The desired MFR (g/s) has been converted to desired flow (g), for a better comparison.

the open-loop tracking error between the desired and the actual mass flow rates were less than 1.06% for sinusoidal, triangular signals, and the square signal, as can be seen in Figure 11.

- At intermediate and high amplitudes and frequencies the errors do not show significant variation for both closed-loop and open-loop cases. Errors between the desired and the actual mass flow were less than 1.52% for all signal types, as can be seen in Figure 11. The error level remained low, thanks to the fact that the benchtop injector can inject liquid up to a rate of 9.8 g/s which was below the experimented flow rates.

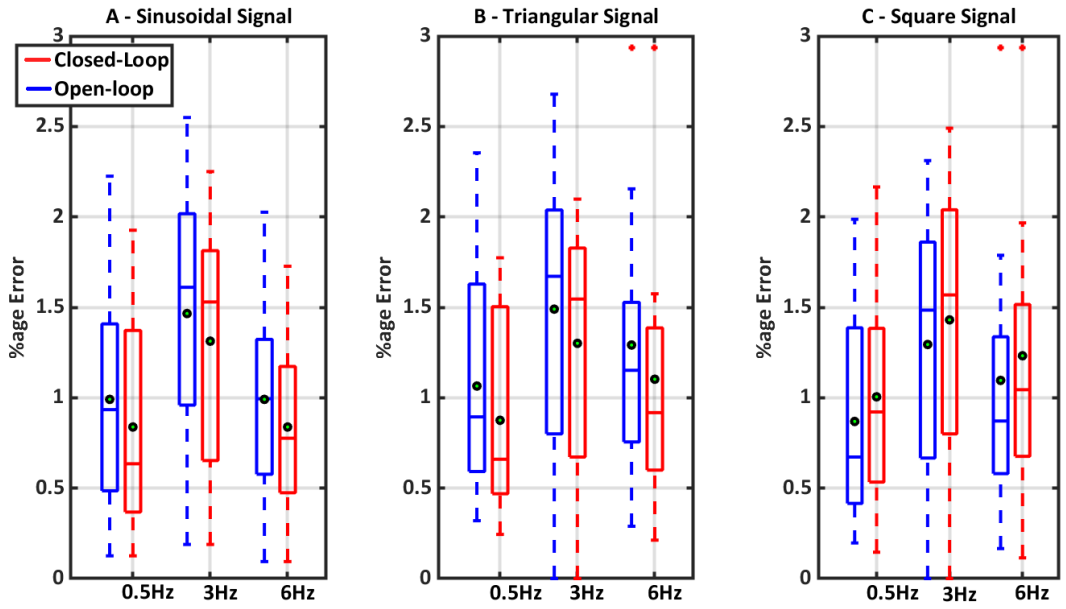

Figure 11. The figure shows the percentage error boxplots for total mass injected as a result of the close- and open-loop control algorithms. (A) shows the tracking result for the sinusoidal reference, (B) for the triangular, and (C) for the square reference signals. Each boxplot shows the respective frequency against the mass flow rate amplitudes of 0.5 g/s, 3 g/s, and 6 g/s. The error percentage was calculated as how much percentage the actual mass flow rate deviates from the desired mass flow rates for 10 trials each. The mean of the trials is also shown with green dots.

- Experiments were also conducted with reference signal frequencies higher than 6 Hz. However, the results were not reported here as satisfactory mass flow rate tracking could not be performed. This was because the injector needle cannot be fully opened following the desired mass flow trajectory at these frequencies. Also, when the flow rate amplitude was large, i.e. $>$9 g/s, the needle cannot move freely between the seating position and the maximum stroke position. Poor performances in these failed cases resulted in mass flow tracking errors of more than 6.8%. These values were accepted as the physical limits of the prototype.

All in all, the designed system works efficiently for low-dosage applications up to 6 Hz. The minimum dosage capabilities can be determined by considering the deadzone time of the solenoid actuator used. Thus, the bandwidth range depends upon the used electromechanical and mechanical components used in the injector system. If a solenoid actuator having a small admittance time is used the efficiency of the applied control algorithm can be further improved. Mechanical design changes can be made by changing the nozzle diameter and plunger mass, using a high-power solenoid, and so on, to increase the bandwidth range.

Conclusion

In this study, a sensorless mass flow rate control for solenoid-based injectors was proposed to be used in the automotive industry. The methodology used yielded successful results, and the desired mass flow injection rates were achieved. The results of the experiments showed that the proposed control method can be used to develop a cost-effective injector for effective dosage applications. As the performance and efficiency of solenoid-based injectors are influenced by the mechanical and electro-mechanical components employed, therefore defining the injector's performance, the industry can achieve optimal functioning injectors via monitoring and adjusting these parameters.

The vital part of this method, as with all injectors that require calibration, is the necessity of accurate calibration to establish the relationship between the position of the needle and the mass flow rate. The calibration process directly affects the controller's performance. In this study, a linear fit was used for the calibration; however, for greater precision, higher-order fits or non-linear models such as look-up tables may be utilized. The main contributions of the study are:

- Position tracking experiments showed less than 2% variation, validating the controller design.
- The mass flow rate tracking achieved an error of less than 1.52%, demonstrating a satisfactory performance.
- The hardware performance was determined to be limited to a flow rate amplitude of $\geq$9 g/s and a reference signal frequency of $\geq$6 Hz, effectively defining its bandwidth.
- Statistical analysis showed that Sensorless Mass Flow Rate Control performed comparably to the controller that used sensor feedback.
- The low standard deviation of the results suggests that the controller used in this study was highly repeatable.

The proposed approach has potential applications in the spray industry, where precise control of injection is essential for complying with new standards and enhancing the performance and efficiency of the system.

References

1. Fabian MM, Hirsch C, Sattelmayer T, Huth M, Meisl J. Investigating the Mixture Quality in Multi-Injector Burner Systems, Part I: Experimental Setup. Journal of Engineering for Gas Turbines and Power. 2022.
2. Wei S, Lee M, Chien Y, Chou T, Wu JS. Experimental investigation of the effect of nozzle throat diameter on the performance of a hybrid rocket motor with swirling injection of high-concentration hydrogen peroxide. Acta Astronautica. 2019;164:334-44.
3. Dong H, Ning B, Cai B, Hou Z. Automatic train control system development and simulation for high-speed railways. IEEE circuits and systems magazine. 2010;10(2):6-18.
4. Wardana MKA, Lim O. Investigation of ammonia homogenization and NOx reduction quantity by remodeling urea injector shapes in heavy-duty diesel engines. Applied Energy. 2022;323:119586.
5. Rodríguez A, Hernández-Herreros N, García JL, Auxiliadora Prieto M. Enhancement of biohydrogen production rate in Rhodospirillum rubrum by a dynamic CO-feeding strategy using dark fermentation. Biotechnology for Biofuels. 2021;14(1):1-16.
6. Xing Z, Hu L, Ripatti DS, Hu X, Feng X. Enhancing carbon dioxide gas-diffusion electrolysis by creating a hydrophobic catalyst microenvironment. Nature communications. 2021;12(1):1-11.
7. Qureshi MS, Kuntuz MP, Bebek O. Performance evaluation of sliding-mode approaches for tracking the motion of the solenoid actuators. In: Int. Conf. On Progresses In Automotive Technologies; 2018. p. 4-14, ISBN: 978-6059546119.
8. Kuntuz MP, Qureshi MS, Bebek O. Sliding Mode Control of an Electromechanical Solenoid Actuator for Soft Landing. In: 23rd International Conference on Methods Models in Automation Robotics (MMAR); 2018. p. 369-74.
9. Qureshi MS, Bebek O. Sensorless position control of solenoid actuators for soft landing using super-twisting sliding mode control. Proceedings of the Institution of Mechanical Engineers, Part D: Journal of Automobile Engineering. 2022:09544070221111617.
10. Bruno N, Zhu Y, Liu C, Gao Q, Li Y. Development of a piezoelectric high speed on/off valve and its application to pneumatic closed-loop position control system. Journal of Mechanical Science and Technology. 2019;33(6):2747-59.
11. Liseli JB, Agnus J, Lutz P, Rakotondrabe M. An Overview of Piezoelectric Self-Sensing Actuation for Nanopositioning Applications: Electrical Circuits, Displacement, and Force Estimation. IEEE Transactions on Instrumentation and Measurement. 2020;69(1):2-14.
12. Pietrzak BW, Le D, Shaver GM. Model-based estimation of piezoelectric fuel injector parameters. In: 2014 American Control Conference; 2014. p. 1529-34.
13. Payri R, Gimeno J, Mata C, Viera A. Rate of injection measurements of a direct-acting piezoelectric injector for different operating temperatures. Energy Conversion and Management. 2017;154:387-93.
14. Dong Q, Yang X, Ni H, Song J, Lu C, Ni Z. An online measurement method of injection rate of high pressure common rail system. Measurement. 2021;170:108716.
15. Coppo M, Dongiovanni C, Negri C. Numerical analysis and experimental investigation of a common rail-type diesel injector. J Eng Gas Turbines Power. 2004;126(4):874-85.
16. Amirante R, Coratella C, Distaso E, Rossini G, Tamburrano P. Optical device for measuring the injectors opening in common rail systems. International Journal of Automotive Technology. 2017;18(4):729-42.
17. Duda K, Wierzbicki S, Śmieja M, Mikulski M. Comparison of performance and emissions of a CRDI diesel engine fuelled with biodiesel of different origin. Fuel. 2018;212:202-22.
18. Ambrosewicz-Walacik M, Wierzbicki S, Mikulski M, Podciborski T. Ternary fuel mixture of diesel, rapeseed oil and tyre pyrolytic oil suitable for modern CRDI engines. Transport. 2018;33(3):727-40.
19. Bartel A. Device and method for controlling an electromagnetic valve; 2010. US Patent 2010/0193719 A1.
20. Lillington R, Chetwynd D, Jones RP. A dynamic model for the drive and electro-mechanics of a solenoid based electronic fuel injector. Proceedings of the Institution of Mechanical Engineers, Part D: Journal of Automobile Engineering. 2019;233(2):199-210.
21. Ming CS, Pai KR. Development of the pneumatic servo control system. In: Proceedings of the JFPS International Symposium on Fluid Power. vol. 2002. The Japan Fluid Power System Society; 2002. p. 11-22.
22. Heister S. Pintle injectors. Handbook of atomization and sprays. 2011:647-55.
23. Melcher JR, Woodson HH. Electromechanical dynamics. Part I: Discrete Systems; John Wiley & Sons, Inc: Hoboken, NJ, USA. 1968.
24. Boizot N, Busvelle E, Gauthier JP. An adaptive high-gain observer for nonlinear systems. Automatica. 2010;46(9):1483-8.
25. Ball A, Khalil H. A nonlinear high-gain observer for systems with measurement noise. IEEE Trans Automat Control. 2013;58:569-80.
26. Derbel N, Ghommam J, Zhu Q. New Developments and Advances in Robot Control. vol. 175. Springer; 2019.
27. Vincent VA, Ahmed-Ali T, Hann C, Lamnabhi-Lagarrigue F. High gain observer design for nonlinear systems with time varying delayed measurements. IFAC Proceedings Volumes. 2011;44(1):692-6.
28. Khalil HK, Grizzle JW. Nonlinear systems. 3rd ed. Prentice Hall, Upper Saddle River, NJ; 2002.
29. Humaidi AJ, Hasan AF. Particle swarm optimization–based adaptive super-twisting sliding mode control design for 2-degree-of-freedom helicopter. Measurement and Control. 2019;52(9-10):1403-19.
30. Nasiri M, Mobayen S, Zhu QM. Super-Twisting Sliding Mode Control for Gearless PMSG-Based Wind Turbine. Complexity. 2019 Apr;2019:1-15.
31. Rivera J, Garcia L, Mora C, Raygoza JJ, Ortega S. Super-twisting sliding mode in motion control systems. Sliding mode control. 2011:237-54.
32. DeCarlo R, Zak S. A quick introduction to sliding mode control and its applications. Dipartimento di ingegneria elettrica ed elettronica, Università degli Studi di Cagliari (Department of Electrical and Electronic Engineering-DIEE, University of Cagliari, Italy). 2008.
33. Park YJ, Kim BG, Jeon JC, Jung D, Choi SB; MDPI. The Effect of Spool Displacement Control to the Flow Rate in the Piezoelectric Stack-Based Valve System Subjected to High Operating Temperature. Actuators. 2021;10(9):239.